# Slow Neutron Resonance Spectroscopy. II. Ag, Au, Ta†

J. S. Desjardins,* J. L. Rosen, W. W. Havens, Jr., and J. Rainwater
*Department of Physics, Columbia University, New York, New York*
(Received August 3, 1960)

The results of time-of-flight measurements of Ag, Au, and Ta resonance parameters are presented. Neutron widths are given for 79 levels in Ag to 728 ev, 55 levels in Au to 940 ev, and 62 levels in Ta to 330 ev. Radiation widths for many of the stronger levels, and in some cases resonance $J$ values are obtained. The reduced neutron width distributions are in good agreement with Porter-Thomas distributions for Au and Ta. The distribution for Ag shows a large excess of small $(2g\Gamma_n{}^0)$ values which are interpreted as $p$-wave resonances and correspond to a $p$-wave strength function $S_1 = (1.7 \pm 0.8) \times 10^{-4}$. The $s$-wave strength functions are $(0.51 \pm 0.09) \times 10^{-4}$ for Ag, $(1.5 \pm 0.3) \times 10^{-4}$ for Au, and $(1.84 \pm 0.34) \times 10^{-4}$ for Ta. The observation of $p$-wave Ag levels is interpreted as due to a $p_{\frac{3}{2}}$ strength function resonance in this region. The level spacing distributions for Au and Ta agree with the expected two-population Wigner spacing distribution function but not with random or single Wigner distributions. The weighted average $\Gamma_\gamma$ values are 0.148 ev, 0.170 ev, and 0.060 ev for Ag, Au, and Ta, respectively.

## I. INTRODUCTION

THIS is the second of what is expected to be a series of papers giving the results of studies using the Columbia University Nevis synchrocyclotron spectrometer system which has been described elsewhere.[1] The first paper of this series,[2] denoted by I, discusses the analysis of self-indication measurements with reference to $U^{238}$ where a single zero-spin isotope is present. In this paper we treat Ag, Au, and Ta where the spin $I$ of the target nucleus is nonzero. For $s$-wave neutrons the compound nucleus spin $J = I \pm \frac{1}{2}$. Aside from the problem of determining the $J$ value for each resonance, the theory of I still applies if one replaces $\Gamma_n$ by $g\Gamma_n$ in the expression for $\sigma_0$ [Eq. (4) of I] to give

$$\sigma_0 = 2.60 E_0^{-1} \times 10^6 (g\Gamma_n/\Gamma) \text{ barns/atom,} \qquad (1)$$

where

$$g = (2J+1)/2(2I+1), \qquad (2)$$

is a spin weight factor. $Au^{197}$ and $Ta^{181}$ are the only stable isotopes of Au and Ta. Ag, however, consists of two almost equally abundant isotopes, $Ag^{107}$ (51.35%) and $Ag^{109}$ (48.65%). For most levels of Ag where the responsible isotope is not known, we make the simplifying assumption that the isotopic sample thickness is one-half that for the element. Ta has $I = \frac{7}{2}$ so $2g = \frac{7}{8}$ $(J=3)$ or 9/8 $(J=4)$. Au has $I = \frac{3}{2}$ so $2g = \frac{3}{4}$ $(J=1)$ or 5/4 $(J=2)$. Both Ag isotopes have $I = \frac{1}{2}$, so $2g = \frac{1}{2}$ $(J=0)$ or $\frac{3}{2}$ $(J=1)$. Since $g\Gamma_n$, rather than $\Gamma_n$, is the best determined quantity, we list values of $2g\Gamma_n$ noting that the average of $2g$ over the two spin values is unity. When the resonance $J$ is known, $2g\Gamma_n$ is easily converted to $\Gamma_n$. Isotope and spin identifications have

previously been made for many of the lower energy Ag levels. The higher spins of Au and Ta make $J$ identifications more difficult for levels of these elements.

In most cases, levels are analyzed assuming $2g=1$ so $\Gamma = \Gamma_\gamma + 2g\Gamma_n$. The analysis then reduces to that described in I with these assumptions and simplifications. Other differences between the $U^{238}$ measurements and those of this paper are mainly favorable to the present measurements and are as follows:

1. Much better peak-to-valley ratios are obtained in the present self-indication measurements due to the absence of the natural sample radioactivity which complicated the $U^{238}$ measurements.

2. For Ag, Au, and Ta self-indication measurements[2a] were made using $D$ only, $D+T_1$, and $D+T_2$. This gives two, rather than one, self-indication transmission values for use in the analysis. The $T_1$ sample was thinner than the $D$ sample, while the $T_2$ sample was of the same, or greater, thickness than the $D$ sample. In the case of Ag, this permitted $J$ to be determined for many levels.

3. We also have flat detector[1] transmission measurements for Au using two transmission samples differing by a factor of 4 in thickness. The two transmission areas provide additional experimental information and permit a better evaluation of level parameters including the determination of many $J$ values. This also provides a valuable cross check of the two techniques.

The systematics of level parameters and spacings have been studied for each element. For Ta and Au the results are consistent with only $s$-wave levels observed, while the Ag results indicate that many $p$-wave levels are also observed. The indicated $p$-wave strength function for Ag is consistent with that found from measurements in the kev region.

[1] J. Rainwater, W. W. Havens, Jr., J. S. Desjardins, and J. L. Rosen, Rev. Sci. Instr. 31, 481 (1960).
[2] J. L. Rosen, J. S. Desjardins, J. Rainwater, and W. W. Havens, Jr., Phys. Rev. 118, 687 (1960).

[2a] For $D$ only a foil of the element is suspended at the detector position (detector sample) and the capture $\gamma$-rays are counted. For $D+T$ a transmission foil ($T$ sample) is *also* present. The method is described in I.
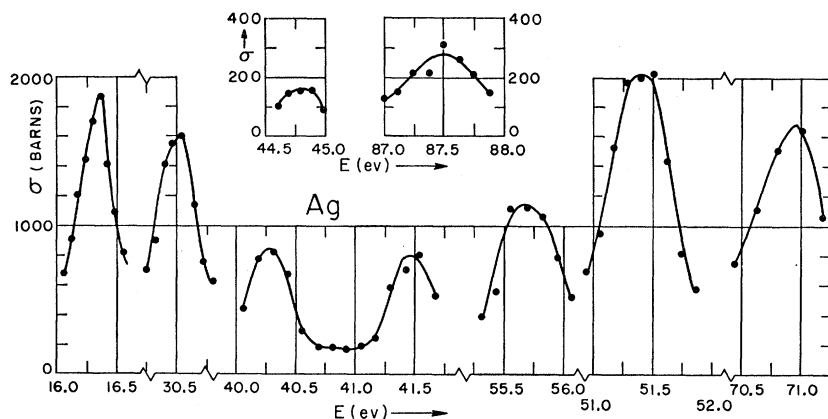
FIG. 1. This shows the self-indication measured (isotopic) cross sections vs energy in the region of the 9 stronger levels between 16 ev and 88 ev. The values result from the transmission ratio of $(D+T)$ to $D$ counts above background after combining groups of channels to obtain better statistical accuracy. The peak values should be essentially equal to $\sigma_A$ for the levels.

## II. MEASUREMENTS AND PRELIMINARY DATA PROCESSING

The measurements were all made using a flight path of $\approx 35$ meters as described in I. In general, 0.1-$\mu$sec detection intervals were used above $\sim 100$ ev and 0.2-$\mu$sec intervals were used below $\sim 100$ ev.

### A. Silver

Self-indication measurements used a foil at the detector position having $(1/n)_D + 103.3$ barns/atom (element). $(D+T_1)$ measurements also used a transmission sample having $(1/n)_{T_1} = 1465$ barns/atom. For $(D+T_2)$ measurements the transmission sample had $(1/n)_{T_2} = 103.3$ barns/atom.

1. For the main run an energy region from 94.6 ev to 1621 ev was studied using 0.1-$\mu$sec detection intervals. About 250 min of total counting time each was spent on the $D$, $D+T_1$, and $D+T_2$ counting.

2. Since analysis of this run indicated the presence of many weak $p$-wave levels, a long $D$ only run was made to obtain better evidence for such levels. This run, using 0.1-$\mu$sec detection intervals and $D$ only, covered the energy region 72.66 ev to 639 ev. About $10^7$ total timed detector counts were obtained in 10 hours of total counting time.

3. A relatively short 0.2-$\mu$sec detection interval run covered the energy region 14.63 ev to 90.5 ev. Total counting times of 92 min, 57 min, and 33 min were devoted to $D$, $D+T_1$, and $D+T_2$, respectively.

### B. Gold

Self-indication and flat detector transmission measurements were made using a variety of sample thicknesses as described below:

1. For the main self-indication measurements the energy region 104.4 ev to 2575 ev was studied using 0.1 $\mu$sec detection intervals. Total counting times of 453 min, 366 min, and 325 min were devoted to $D$, $D+T_1$, and $D+T_2$, respectively, with $(1/n)_D = 213$ barns/atom, $(1/n)_{T_1} = 426$ barns/atom, and $(1/n)_{T_2} = 106.5$ barns/atom.

2. For the main flat-detector transmission measurements the energy region 99.1 ev to 2024 ev was studied using 0.1-$\mu$sec detection intervals. Total counting times of 639 min, 320 min, and 320 min were devoted to open, $T_1$, and $T_2$, respectively. The same transmission samples as above were used.

3. Self-indication measurements were made using 0.2-$\mu$sec detection intervals for the region 15.86 ev to 111 ev. Only $D$ and $D+T_1$ measurements were made where both samples had $(1/n) = 426$ barns/atom. A total counting time of 46 min was devoted to each condition.

### C. Tantalum

Two series of $D$, $D+T_1$, and $D+T_2$ measurements were made with 0.1-$\mu$sec detection intervals covering the region 75.1 ev to 717 ev. The two series used the same sample thicknesses and were analyzed separately as a consistency check. Total counting times of about 223 min, 259 min, and 266 min were devoted to $D$, $D+T_1$, and $D+T_2$, respectively. The samples had $(1/n) = 140$, 700, and 140 barns/atom for the $D$, $T_1$, and $T_2$ samples, respectively.

Each of the above series of measurements on Ag, Au, and Ta represent a number of cycles of $\sim 30$ min for each condition. In addition, several short cycles were made for each series to establish the relative $D$, $D+T_1$, $D+T_2$ counting rates for constant cyclotron intensity for normalization purposes.

The initial processing of the data was made for each series as in I. Transmission values were calculated corresponding to the total $\sigma$ and to $\sigma$ minus the potential scattering, $\sigma_p$.

## III. ANALYSIS AND RESULTS

### A. Silver

The main Ag resonances below 100 ev have been carefully studied previously,[3] particularly by the

[3] See *Neutron Cross Sections*, compiled by D. J. Hughes and R. Schwartz, Brookhaven National Laboratory Report BNL-325 (Superintendent of Documents, U. S. Government Printing Office, Washington, D. C., 1958), 2nd ed., for a review of earlier neutron cross-section studies.

TABLE I. Resonance parameters for Ag. The values for $2g\Gamma_n$, etc., are for the isotope, assuming equal abundances of $Ag^{107}$ and $Ag^{109}$ in natural Ag. Although isotope assignments are given in BNL-325 for 11 levels to 134 ev, our analysis is independent of isotope assignment. The $J$ assignments and $\Gamma_\gamma$ values below 100 ev, and the parameters for the 5.2-ev level are from BNL-325. All other energies, spins, and level widths are based on the present measurements. The levels denoted by asterisks were considered to be $p$ wave and the corresponding $2g\Gamma_n^1$ are given. These levels appear in the $(2g\Gamma_n^1)$ distribution of Fig. 5. The $2g\Gamma_n^1$ values were calculated using $R=1.35A^{\frac{1}{3}}\times10^{-13}$ cm for the nuclear radius. Uncertain $J$ assignments are enclosed in parentheses.

| $E_0$ (ev) | $2g\Gamma_n$ ($10^{-3}$ ev) | $\Gamma_\gamma$ ($10^{-3}$ev) | $J$ | $2g\Gamma_n^0$ ($10^{-3}$ ev) | $2g\Gamma_n^1$ ($10^{-3}$ ev) |
|---|---|---|---|---|---|
| 5.2±0.01 | 18.8±0.15 | 140±3 | 1 | 8.17±0.06 | |
| 16.3±0.03 | 6.0±0.3 | 140±8 | 0 | 1.48±0.07 | |
| 30.5±0.06 | 11.0±1.0 | 125±13 | 1 | 2.0±0.18 | |
| 40.2±0.08 | 8.6±1.0 | 137±19 | 1 | 1.35±0.16 | |
| 41.5±0.08 | 8.5±1.0 | 148±11 | 1 | 1.32±0.16 | |
| 44.8±0.08 | 1.80±0.25 | | | 0.27±0.04 | |
| 51.4±0.1 | 33±3 | 128±10 | 1 | 4.47±0.41 | |
| 55.7±0.1 | 19.0±1.5 | 144±11 | 0 | 2.56±0.20 | |
| 70.8±0.1 | 42±4 | 120±40 | 1 | 4.76±0.45 | |
| *82.4±0.2 | 0.03±0.006 | | | 0.0033±0.0007 | 21 |
| *83.5±0.2 | 0.04±0.01 | | | 0.003±0.0008 | 14 |
| 87.4±0.2 | 9.3±0.7 | 140±21 | 0 | 0.99±0.07 | |
| *91.5±0.2 | 0.05±0.01 | | | 0.005±0.001 | 27 |
| *106.3±0.2 | 0.22±0.03 | | | 0.022±0.003 | 104 |
| *110.7±0.2 | 0.11±0.02 | | | 0.011±0.002 | 52 |
| *128.4±0.2 | 0.15±0.03 | | | 0.012±0.002 | 50 |
| 133.9±0.3 | 125±8 | 137±10 | 1 | 10.9±0.7 | |
| 139.9±0.3 | 2.0±0.5 | | | 0.17±0.04 | |
| 144.3±0.3 | 8.5±1.0 | 129±15 | (0) | 0.71±0.08 | |
| *155.0±0.3 | 0.09±0.03 | | | 0.008±0.002 | 25 |
| *162.0±0.3 | 0.30±0.08 | | | 0.024±0.005 | 104 |
| *167.0±0.3 | 0.26±0.05 | | | 0.02±0.004 | 62 |
| *169.8±0.3 | 0.22±0.04 | | | 0.018±0.004 | 53 |
| 173.4±0.3 | 84±10 | 170±25 | 1 | 6.4±0.8 | |
| *183.7±0.4 | 0.28±0.06 | | | 0.021±0.004 | 59 |
| 202.9±0.4 | 23±3 | 154±15 | 1 | 1.6±0.2 | |
| 209.0±0.4 | 32±3 | 157±15 | 1 | 2.2±0.2 | |
| *218.2±0.4 | 0.17±0.03 | | | 0.011±0.002 | 28 |
| *228.7±0.5 | 0.07±0.02 | | | 0.005±0.001 | 10 |
| 251.7±0.5 | 42±4 | 168±20 | 1 | 2.64±0.25 | |
| 259.4±0.5 | 3.2±0.4 | | | 0.2±0.025 | |
| 265.0±0.5 | 5.0±0.8 | | | 0.31±0.05 | |
| *270.4±0.5 | 0.047±0.02 | | | 0.0028±0.0012 | 5 |
| 273.0±0.5 | 2.8±0.4 | | | 0.17±0.02 | |
| 284.5±0.6 | 0.53±0.10 | | | 0.031±0.006 | |
| 291.0±0.6 | 18±2 | 134±15 | 0 | 1.05±0.12 | |
| *293.8±0.6 | 0.27±0.05 | | | 0.016±0.003 | 29 |
| *296.9±0.6 | 0.19±0.04 | | | 0.011±0.002 | 19 |
| 300.9±0.6 | 2.0±0.5 | | | 0.115±0.029 | |
| 311.0±0.6 | 167±40 | | | 9.5±2.3 | |
| 316.7±0.6 | 250±50 | | | 14.1±2.8 | |
| 328 ±0.7 | 10.0±1.5 | | | 0.55±0.08 | |
| *340 ±0.7 | 0.37±0.07 | | | 0.020±0.004 | 30 |
| 347 ±0.7 | 0.79±0.2 | | | 0.042±0.011 | |
| 362 ±0.7 | 32±3 | 175±25 | 1 | 1.68±0.16 | |
| 374 ±0.7 | 1.3±0.2 | | | 0.067±0.010 | |
| 388 ±0.8 | 57±5 | 180±30 | 1 | 2.9±0.25 | |
| *392 ±0.8 | 0.16±0.03 | | | 0.0081±0.0015 | 10 |
| 398 ±0.8 | 36±4 | 150±30 | (1) | 1.8±0.2 | |
| 405 ±0.8 | 80±5 | 153±15 | 0 | 3.97±0.25 | |
| 410 ±0.8 | 0.95±0.02 | | | 0.047±0.001 | |
| 429 ±0.9 | 17±3 | | | 0.82±0.14 | |
| 446 ±0.9 | 28±3 | 136±15 | 1 | 1.32±0.14 | |
| 462 ±0.9 | ~40 | | | ~18.6 | |
| 467 ±0.9 | ~120 | | | ~5.6 | |
| 469 ±0.9 | ~60 | | | ~2.8 | |
| 480 ±1.0 | 0.33±0.07 | | | 0.015±0.003 | |
| 489 ±1.0 | 24±5 | | | 1.08±0.23 | |
| 502 ±1.0 | 330±35 | 130±15 | 1 | 14.7±1.6 | |
| 512 ±1.0 | 20±10 | | | 0.88±0.44 | |
| 515 ±1.0 | 90±40 | | | 3.96±1.76 | |
| 526 ±1.0 | 5.7±0.7 | | | 0.25±0.03 | |
| 532 ±1.1 | 0.88±0.25 | | | 0.038±0.011 | |
| 544 ±1.1 | ~1 | | | ~0.04 | |
| 555 ±1.1 | ~70 | | | ~3.0 | |
| 561 ±1.1 | ~30 | | | ~1.3 | |
| 567 ±1.1 | ~50 | | | ~2.1 | |
| 577 ±1.2 | 42±10 | 127±20 | (1) | 1.75±0.42 | |
| 588 ±1.2 | 90±10 | 142±15 | 1 | 3.71±0.41 | |
| 609 ±1.2 | 43±8 | 150±30 | 1 | 1.74±0.32 | |
| 622 ±1.2 | ~60 | | | ~2.4 | |
| 628 ±1.3 | ~10 | | | ~0.4 | |
| 634 ±1.3 | 1.1±0.3 | | | 0.044±0.012 | |
| 655 ±1.3 | 17±3 | | | 0.66±0.12 | |
| 669 ±1.4 | ~80 | | | ~3.1 | |
| 678 ±1.4 | ~120 | | | ~4.6 | |
| 685 ±1.4 | 2±1 | | | 0.076±0.038 | |
| 698 ±1.4 | 26±10 | | | 0.985±0.379 | |
| 705 ±1.5 | 4±2 | | | 0.15±0.08 | |
| 728 ±1.5 | ~35 | | | ~1.3 | |

Harwell group,[4] so our relatively short run in this region was mainly intended to establish the resonance energies more precisely. Since a relatively large number of detection intervals are involved for each resonance, it proved possible to combine groups of detection intervals to improve the statistical accuracy of each point yet still have many points define each resonance. Since the resolution width is small compared to the Doppler broadened level widths in this region, we have plotted measured cross sections vs energy in Fig. 1. These were obtained in the usual manner by taking the ratio of $(D+T)$ to $D$ counts (above background) to give an experimental transmission. Note that the peaks of the curves essentially give $\sigma_A$. Since $\Delta$ is a priori known, $\sigma_0\Gamma$, and thus $2g\Gamma_n$, was calculated from $\sigma_A\Delta$ using Eq. (6) of I. The spin assignments of BNL-325 were

[4] E. R. Rae, E. R. Collins, B. B. Kinsey, J. E. Lynn, and E. R. Wiblin, Nuclear Phys. 5, 89 (1958).

used, with $\Gamma_\gamma=0.140$ ev to obtain $\Gamma/\Delta$. The result is relatively insensitive to moderate changes in $\Gamma$.

Table I lists the results for the Ag level parameters for all levels studied. The results for the 5.2-ev level are from BNL-325 and those for the levels not shown in Fig. 1 are from our other Ag series of measurements. Figure 2 shows the results below 1000 ev for the main 0.1-$\mu$sec detection interval Ag run.

Figure 3 shows the running sum of the number of observed Ag levels (both isotopes) vs energy. The shape of the plot suggests that relatively few levels are missed to 575 ev, but that a significant fraction of the levels are missed above 575 ev as reflected by the decreasing slope. The observation of many $p$-wave levels, as discussed below, somewhat confuses this interpretation. In Fig. 2 there are many very weak resonance peaks in the $D$, $D+T_1$, and $D+T_2$ curves which seem to belong to a different population than

the other levels. Examples are the peaks at 106.3 ev, 110.7 ev, 128.4 ev, 162 ev, 167 ev, and 183.7 ev. To provide a more stringent search for such levels a long $D$ only run was made covering the energy range from 72.66 ev to 693 ev as described in the preceding section. The plot of this run is not given, but it was very useful in detecting and confirming the presence of these weak levels.

In evaluating level parameters, three basic bits of information are available for each level. They are the two self-indication transmission values $(T_{SI})_1$ and $(T_{SI})_2$ and the total number of counts $C$ above background in the $D$-only resonance peak. As discussed in I, one also determines, from a collective first analysis of the levels, a value of $S_a = (\Gamma/\Gamma_\gamma)S_r$, where $S_r$ is the (unknown) count per channel corresponding to $T=0$ for the $D$ sample. The use of the $T_{SI}$ values, which represent the ratio of total $D+T$ to $D$-only level counts, is described in I together with one way of using $C$ and $S_a$. A new method, described below, has been developed for using $C$ and $S_a$ independent of the $T_{SI}$ results. If $\delta E =$ the energy spacing per channel, then

$$A \equiv \int (1-T)dE = A_0\Gamma/\Gamma_\gamma, \qquad (3)$$

where $A_0 \equiv C\delta E/S_a$ is known. This can be written as $\Gamma_n = (\Gamma - \Gamma_\gamma) = \Gamma(1 - A_0/A)$ which, when inserted into Eq. (1) gives

$$n\sigma_0 = Fg(1 - A_0/A). \qquad (4)$$

Here $F = 2.60nE_0^{-1} \times 10^6$ and $A_0$ are known, while $g$ can be either $g_+$ or $g_-$ corresponding to $J = I \pm \frac{1}{2}$. A figure was constructed giving plots of $A/\Delta$ vs $n\sigma_0$ with one curve for each choice of $\Delta/\Gamma$. This is called the "standard analysis figure" and is applicable to all levels. For a given level, a transparent overlay is placed over this figure and two separate curves are constructed using Eq. (4) for $g_+$ and for $g_-$. The intersections of the standard analysis curve corresponding to a given choice of $\Delta/\Gamma$ and the curve for $g_+$ determine compatible pairs of $\Gamma$, $n\sigma_0$ values for $g_+$. Repeating for other $\Delta/\Gamma$ values, one obtains a plot $n\sigma_0$ or $g\Gamma_n$ vs $\Gamma$ for $g_+$. A plot for $g_-$ is similarly obtained.

Figure 4(a), (b), (c), (d) give examples of the analysis for the levels at 134 ev, 405 ev, 502 ev, and 588 ev. The two $T_{SI}$ values give relations between $g\Gamma_n$ and $\Gamma$ independent of $J$. The curves labeled $J=0$ and $J=1$ are those determined from $C$ and $S_a$.

In those cases where only one of these curves is consistent with the $T_{SI}$ curves, the choice of $J$ as well as $g\Gamma_n$ and $\Gamma$ are well defined [Figs. 4(a), (c)]. In any event, an additional test is made that the predicted $\Gamma_\gamma$ is reasonably near to the average $\Gamma_\gamma \approx 0.140$ ev for those levels where $\Gamma_\gamma$ is accurately determined. For most cases only the $(T_{SI})_2$ curve is accurate because $(T_{SI})_1$ is too near unity and the favored $J$ is that which gives a reasonable value of $\Gamma_\gamma$. In Fig. 4(d), for example, the

$J=0$ intersection gives $\Gamma_\gamma = 0.252$ ev, while the favored $J=1$ intersection gives $\Gamma_\gamma = 0.142$ ev. In Fig. 4(b), the choice of $J$ is also made mainly on the basis of the predicted $\Gamma_\gamma$, which is $\approx 0.153$ ev for the favored $J=0$ choice and $\approx 0.087$ ev for $J=1$. In the case of a still weaker level, where $\Gamma_\gamma \gg \Gamma_n$, the two curves for different
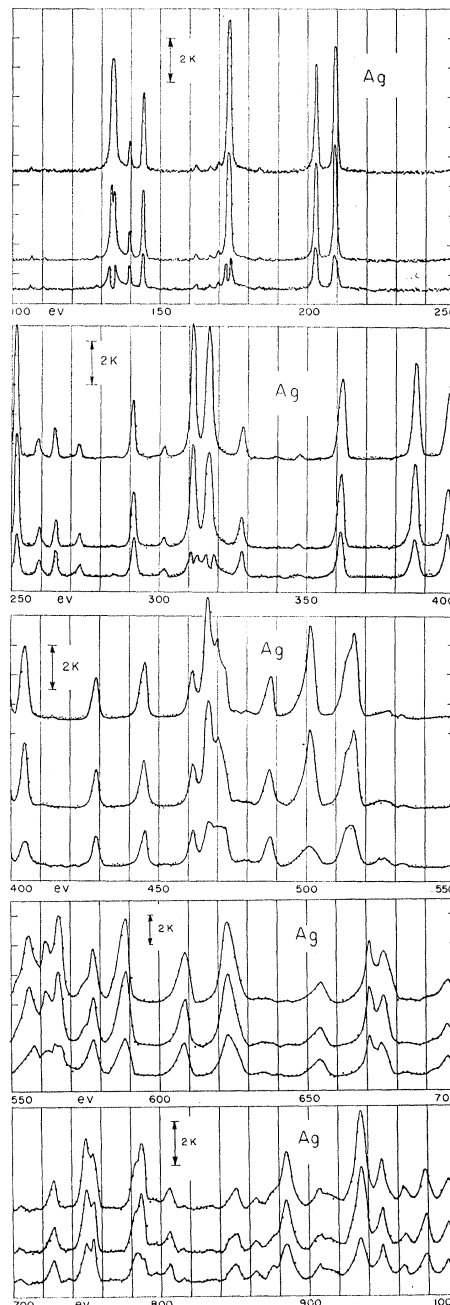


FIG. 2. Self-indication $\gamma$ ray counts per 0.1-$\mu$sec detection interval for Ag. The curves have a smooth background function subtracted and are displaced vertically by arbitrary amounts for clarity. The vertical displacement corresponding to 2000 counts per channel is indicated. The $D$, $T_1$, and $T_2$ samples have $n^{-1}$ of 103.3, 1465, and 103.3 barns/atom (element), respectively.
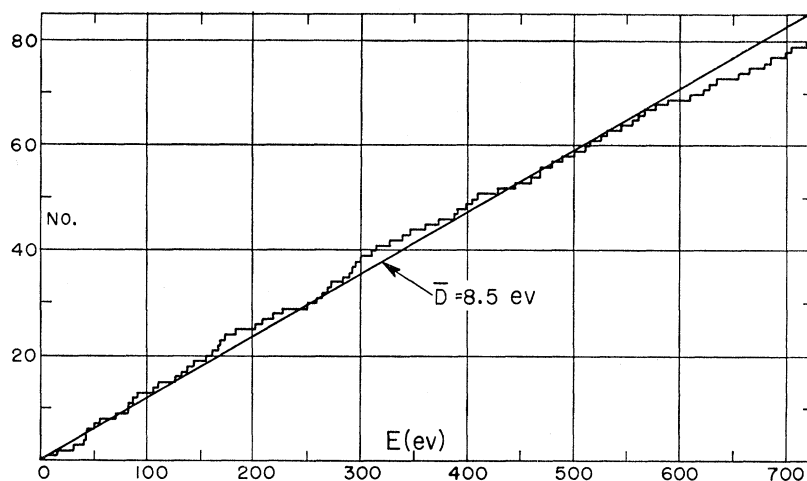
FIG. 3. The number of observed resonances in normal Ag to energy $E$ vs $E$. The slope of the curve yields the average level spacing and indicates the energy ($\sim$575 ev) above which a significant fraction of the levels are missed.

$J$ resulting from the $D$-only curve and the $S_a$ value tend to be indistinguishable and insensitive to $\Gamma$. $(T_{SI})_2$ may also be too close to unity to be useful, and in any case tends to give $g\Gamma_n$ relatively independent of $\Gamma$. An inspection of Table I shows that $J$ values for levels above 100 ev have been obtained only for relatively strong levels (large $2g\Gamma_n$) which are sufficiently well separated in energy from neighboring levels.

The integral distribution of reduced neutron widths $2g\Gamma_n{}^0$ is plotted against $(2g\Gamma_n{}^0)^{\frac{1}{2}}$ in Fig. 5 for the first 53 levels to 447 ev. A single Porter-Thomas curve normalized to this number of levels shows a poor agreement with the experimental curve in a way that suggests that many of the weak levels belong to a different distribution and should be ignored in attempting to obtain an $s$-wave fit. In view of this, two additional theoretical distributions are indicated in Fig. 5

based on 36 and 40 total $s$-wave levels which are to be compared with the experimental distribution everywhere except in the region of very weak levels.

To investigate the possibility that these weak levels might be due to impurities, two approaches were followed: (1) A spectrochemical analysis was performed for a representative list of possible contaminants. This included tests for Cd, Ta, Pt, Hg, Sb, and Au. The results were all negative with a sensitivity limit of 0.04% or smaller. Concentrations of Cu of $\sim$0.01% and Zn of $\sim$0.001% were found, however. (2) As a second test, the positions, widths, and relative strengths of the weak levels were compared with all the data tabulated in BNL-325 in a search for a consistent pattern of agreement with the strong levels listed there. This also yielded negative results subject to the limitations in completeness of the data in BNL-325.
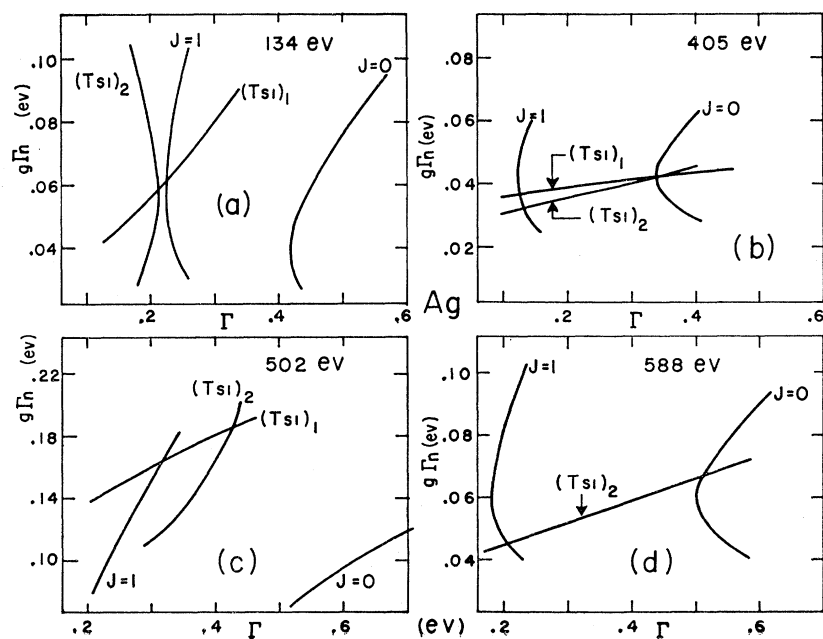


FIG. 4. Examples for Ag of the self-indication method of level analysis. Each $T_{SI}$ value determines one curve of $g\Gamma_n$ vs $\Gamma$. Two other curves are also determined one for each $J$ choice, from the total counts $C$ above background in the $D$-only resonance peak and a knowledge of $S_a$. The method of constructing these curves is described in the text.
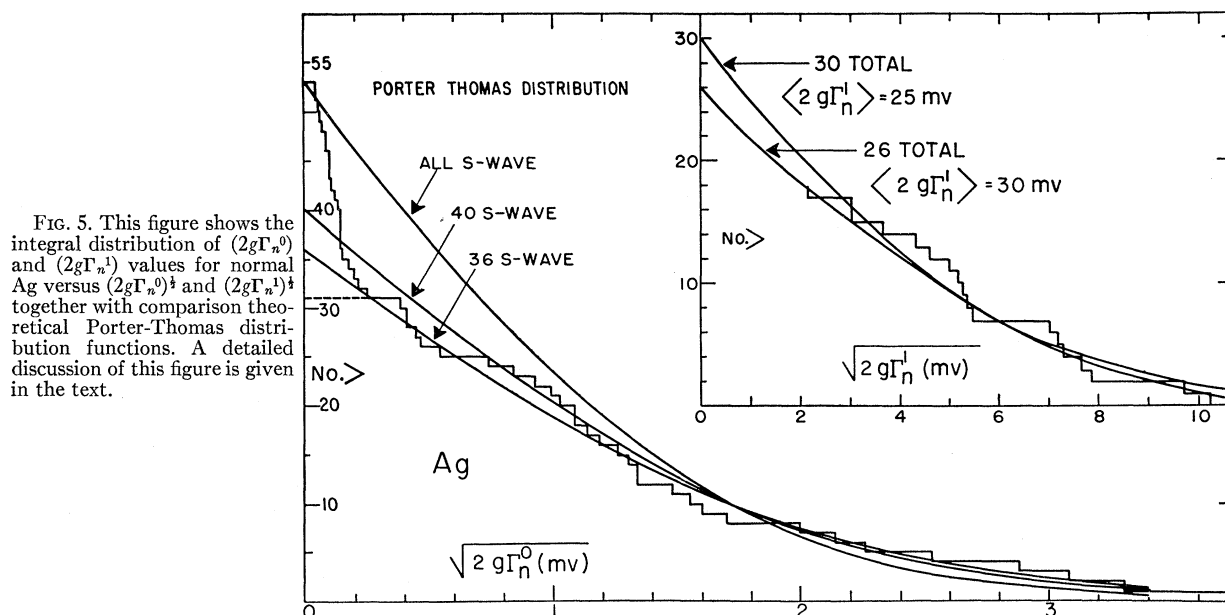
FIG. 5. This figure shows the integral distribution of $(2g\Gamma_n{}^0)$ and $(2g\Gamma_n{}^1)$ values for normal Ag versus $(2g\Gamma_n{}^0)^{\frac{1}{2}}$ and $(2g\Gamma_n{}^1)^{\frac{1}{2}}$ together with comparison theoretical Porter-Thomas distribution functions. A detailed discussion of this figure is given in the text.

It thus appears very unlikely that the weak levels are due to impurities in the sample.

As discussed in I [see the Introduction, and Eqs. (13) and (14) and the associated discussion], one expects $p$-wave levels to be present with $g\Gamma_n$ values smaller than for $s$-wave levels by a factor of approximately $S_1 x^2 [(1+x^2)S_0]^{-1}$, where $S_0$ and $S_1$ are the $s$- and $p$-wave strength functions and $x^2 = E_0/E_1$, where $E_1$ is the energy at which the neutron $\lambda$ equals the nuclear radius $R$ (approximately equal to 500 kev for Ag). $S_0$ and $S_1$ are expected to be $\approx 10^{-4}$ but show long range resonance variations with nuclear size in agreement with the predictions of a realistically sophisticated optical model. In particular, Ag is in a region of an expected minimum for $S_0$ and maximum for $S_1$. There is evidence[5] for an expected spin orbit splitting with

the peak in the $p_{\frac{3}{2}}$ strength function near $A = 92$ and the peak in the $p_{\frac{1}{2}}$ strength function near $A = 111$. For $A = 107$ or 109 only the $p_{\frac{1}{2}}$ peak should contribute appreciably.

The first report of a probable observation of many $p$-wave resonances for $E_0 < 1000$ ev was given by Saplakoglu et al.[6] for $Nb^{92}$ which is at the peak of the $p_{\frac{3}{2}}$ strength function region. They classified about $\frac{2}{3}$ of the observed levels as $p$ levels and $\frac{1}{3}$ as $s$ levels. This is the expected $p_{\frac{3}{2}}$ to $s$ statistical factor for relative level abundance if one assumes a $(2l+1)$ relative level density (for low $l$ where the Gaussian factor is nearly unity) for all states, whether observed or not, accessible to neutrons of a given $l$. If a $(2J+1)$ relative weighting is assigned to states of each $J$ associated with $s_{\frac{1}{2}}$, $p_{\frac{1}{2}}$, and $p_{\frac{3}{2}}$ wave neutrons, then the relative density of
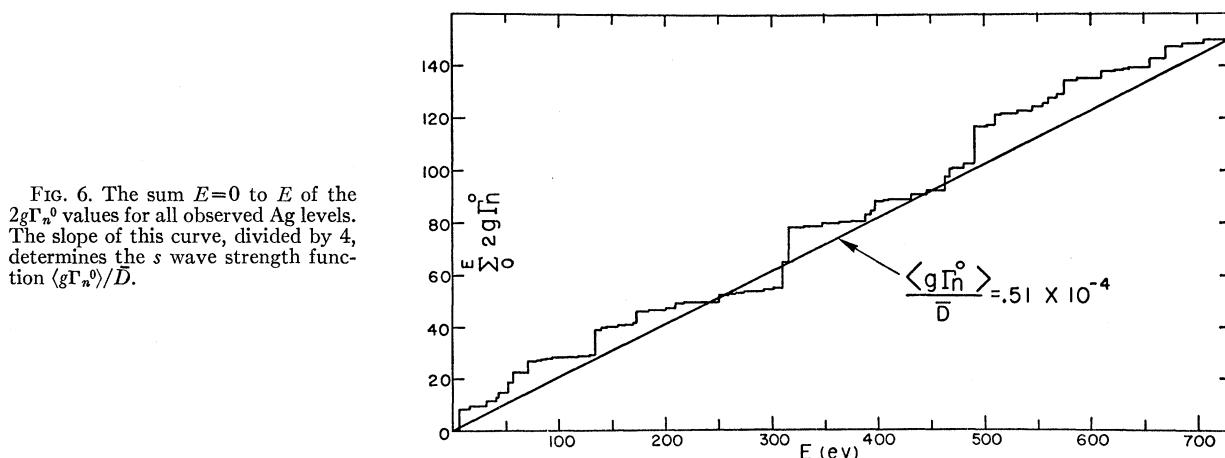
FIG. 6. The sum $E=0$ to $E$ of the $2g\Gamma_n{}^0$ values for all observed Ag levels. The slope of this curve, divided by 4, determines the $s$ wave strength function $\langle g\Gamma_n{}^0 \rangle / \bar{D}$.

[5] See the figure and discussion of K. Seth Proceedings of the International Conference on the Nuclear Optical Model, Florida State University Studies, No. 32 (The Florida State University, Tallahassee, Florida, 1959), pp. 175–176.

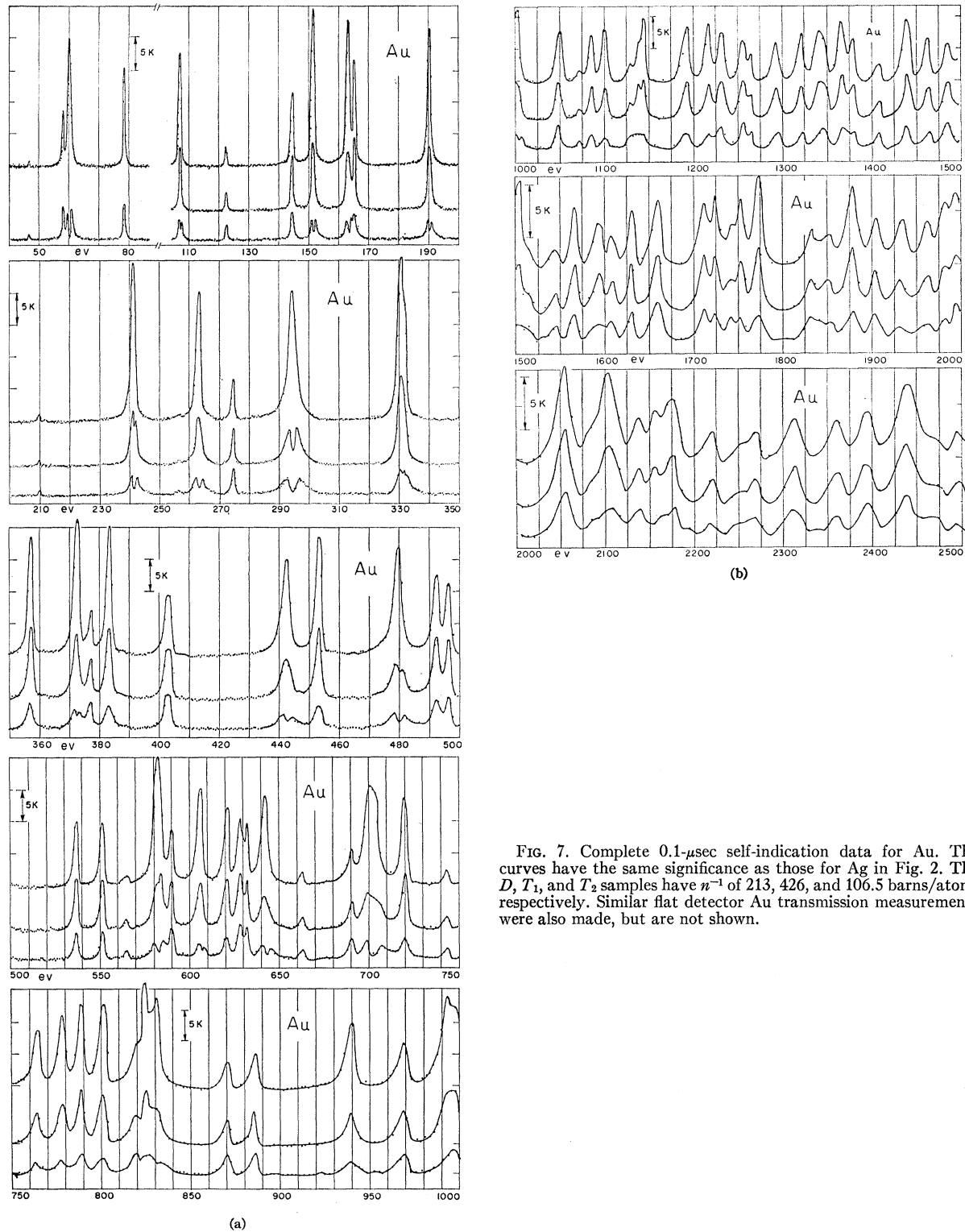[6] A. Saplakoglu, L. M. Bollinger, and R. E. Coté, Phys. Rev. 109, 1258 (1958).

(a)



(b)

FIG. 7. Complete 0.1-$\mu$sec self-indication data for Au. The curves have the same significance as those for Ag in Fig. 2. The $D$, $T_1$, and $T_2$ samples have $n^{-1}$ of 213, 426, and 106.5 barns/atom, respectively. Similar flat detector Au transmission measurements were also made, but are not shown.

levels accessible to $s_{\frac{1}{2}}$, $p_{\frac{1}{2}}$, and $p_{\frac{3}{2}}$ neutrons should be as 1, 1, and 2. It is possible that some of the levels which can be induced by $p_{\frac{1}{2}}$-wave neutrons can also be induced by $p_{\frac{3}{2}}$-wave neutrons if they have the same $J$ and parity. This would confuse the above counting.

A study of Table I and Fig. 5 suggests that one may

say that essentially all levels having $2g\Gamma_n^0 \geq 0.015$ are probably $s$-wave levels. The next $2g\Gamma_n^0$ value is 0.011 and from here down most of the levels are believed to be $p$ levels. In comparing the experimental and Porter-Thomas distributions of $(2g\Gamma_n^0)^{\frac{1}{2}}$ values, the region $(2g\Gamma_n^0)^{\frac{1}{2}} \geq 0.38$, having 31 levels, should be emphasized. The theoretical curve normalized to 36 levels gives a good fit and suggests that $\sim 5$ levels having $(2g\Gamma_n^0)$ $\leq 0.011$ are $s$ wave. The insert shows the corresponding $p$-wave distribution of $(2g\Gamma_n^1)^{\frac{1}{2}}$ values using the 18 levels between 80 ev and 447 ev indicated by asterisks in Table I. Four weak levels were arbitrarily omitted to give a proper subtraction of weak $s$-wave levels. This region is expected to contain about 26 $s$ levels and it is interesting to note that the best fit to the $(2g\Gamma_n^1)$ distribution requires about the same total number of $p$ levels, with about 10 of the weakest $p$ levels assumed missed.

It is clear from Fig. 6, which shows the sum of the $(2g\Gamma_n^0)$ values vs $E$, that the removal of the weak
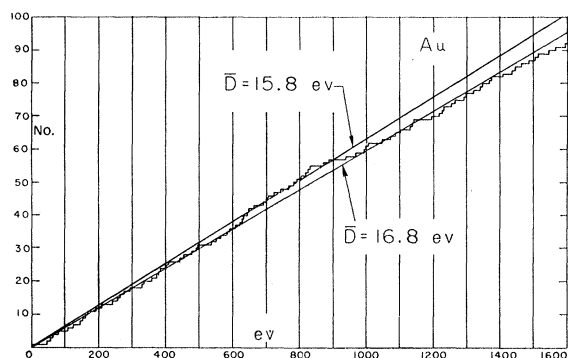


FIG. 8. The number of levels to energy $E$ vs $E$ for Au. Two possible choices of $\bar{D}$ are indicated as discussed in the text.

levels described above will not significantly alter the experimentally determined $S_0$ of

$$S_0 \equiv (\Delta E)^{-1} \sum_{(\Delta E)} (g\Gamma_n^0) = \langle g\Gamma_n^0 \rangle / \bar{D}_0$$

$$= (0.51 \pm 0.09) \times 10^{-4}. \tag{5}$$

The stated uncertainty is essentially all due to statistical considerations concerning the number, $n$, of levels sampled. If $n$ levels are observed, the expected fractional fluctuation in $\Sigma(g\Gamma_n^0)$ is $(2/n)^{\frac{1}{2}}$ if the two spin states have the same Porter-Thomas distribution of $(g\Gamma_r^0)$ values. For random level spacings, the fractional fluctuation (rms) expected in the number of levels observed in a given (large) energy interval is $(1/n)^{\frac{1}{2}}$ while $[(4-\pi)/\pi n]^{\frac{1}{2}}$ applies for a single-population Wigner spacing function. Combining these contributions in quadrature gives a net fractional uncertainty of $1.5n^{-\frac{1}{2}}$ to $1.7n^{-\frac{1}{2}}$, based only on the size of the sample, for the two extreme spacing distributions.
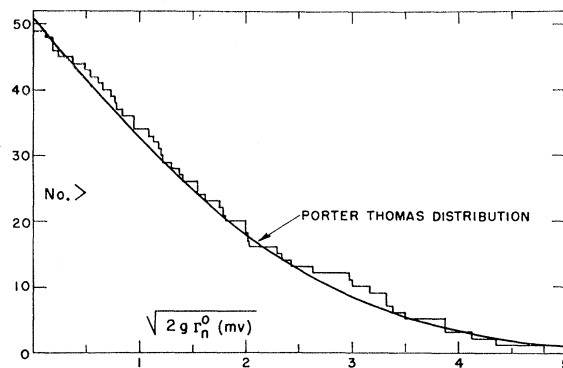


FIG. 9. Integral distribution of the reduced width amplitudes $(2g\Gamma_n^0)^{\frac{1}{2}}$ for Au for the first 49 levels to 800 ev. A comparison good-fit Porter-Thomas function is shown normalized to 2 extra levels.

Failure to include a few weak levels does not significantly alter this result.

There are many alternate ways of treating $s$- and $p$-wave strength functions. For $s$ waves one may use an effective net $S_0$ as in Eq. (5) where $\bar{D}_0$ is the average $s$ level spacing. For $I \neq 0$ one may also consider separately the $s$-wave strength functions for $I - \frac{1}{2}$ and $I + \frac{1}{2}$ $s$-wave states. For $p$-wave states one may use a net $p$-wave strength function $S_1$ as defined in Eq. (14) of I, or one may consider separate strength functions for $p_{\frac{1}{2}}$ and $p_{\frac{3}{2}}$ neutrons. A further division is possible if separate strength functions are used for states of each possible $J$ for both $p_{\frac{1}{2}}$ and $p_{\frac{3}{2}}$. For the case where separate $p_{\frac{1}{2}}$ and $p_{\frac{3}{2}}$ strength functions $(S_1)_{\frac{1}{2}}$ and $(S_1)_{\frac{3}{2}}$ are to be defined, Eqs. (13) and (14) of I, while still applying for the net $S_1$, become

$$\langle \sigma_c^1 \rangle = 2\pi^2 \lambda^2 E^{\frac{1}{2}} \left( \frac{x^2}{1+x^2} \right) [(S_1)_{\frac{1}{2}} + 2(S_1)_{\frac{3}{2}}]$$

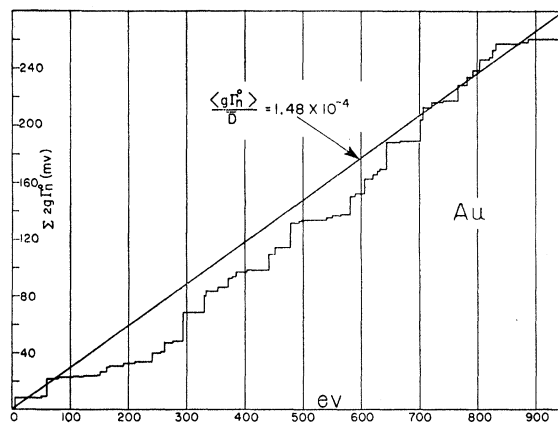$$= 2\pi^2 \lambda^2 (\Delta E)^{-1} \sum_p (g\Gamma_n^1), \tag{6}$$



FIG. 10. The sum $E=0$ to $E$ of the $2g\Gamma_n^0$ values for Au to 940 ev. The slope divided by 2 determines the Au strength function.
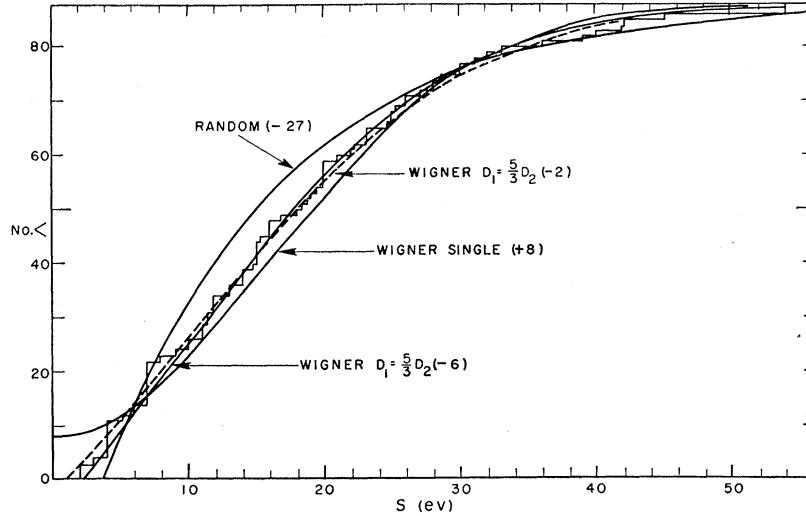
FIG. 11. Integral distribution of Au level spacings for the 88 observed spacings to 1566 ev. Four theoretical curves are drawn for comparison. The total number of spacings has been adjusted for a best fit in each case by assuming that the missing (or excess) levels occur in the region of small level spacings. The Wigner two population curves $(D_1=5D_2/3)$ are for 90 and 94 total levels, with $y$ intercepts of $-2$ and $-6$, respectively, as indicated. Equally good fits can be obtained using $\bar{D}_1=D_2$ but the random and single Wigner fits are poor.

where

$$(S_1)_{\frac{1}{4}} \equiv (\Delta E)^{-1} \sum_{p_{\frac{1}{2}}} (g\Gamma_n{}^1) = \langle g\Gamma_n{}^1 \rangle_{\frac{1}{2}}/\bar{D}_{1,\frac{1}{2}} \qquad (7a)$$

$$2(S_1)_{\frac{3}{4}} \equiv (\Delta E)^{-1} \sum_{p_{\frac{3}{2}}} (g\Gamma_n{}^1) = \langle g\Gamma_n{}^1 \rangle_{\frac{3}{2}}/\bar{D}_{1,\frac{3}{2}} \qquad (7b)$$

$$3S_1 \equiv (\Delta E)^{-1} \sum_{p} (g\Gamma_n{}^1) = (S_1)_{\frac{1}{4}} + 2(S_1)_{\frac{3}{4}}, \qquad (7c)$$

with $\Gamma_n{}^1$ defined as in I.

An energy interval $\Delta E$ is assumed over which one sums the contribution of all $p_{\frac{1}{2}}$ induced levels (7a), all $p_{\frac{3}{2}}$ induced levels (7b), or all $p$ induced levels (7c). The numbers of $p_{\frac{1}{2}}$, $p_{\frac{3}{2}}$, and total $p$ induced levels are inversely proportional to $\bar{D}_{1,\frac{1}{2}}$, $\bar{D}_{1,\frac{3}{2}}$, and $\bar{D}_1$, respectively. If some levels can be excited both by $p_{\frac{1}{2}}$ and $p_{\frac{3}{2}}$ neutrons, one should, in principle, count them only once in (7c) and divide them somehow between (7a) and (7b). (This might be done on the basis of the relative strength of their $p_{\frac{1}{2}}$ and $p_{\frac{3}{2}}$ wave excitations.)

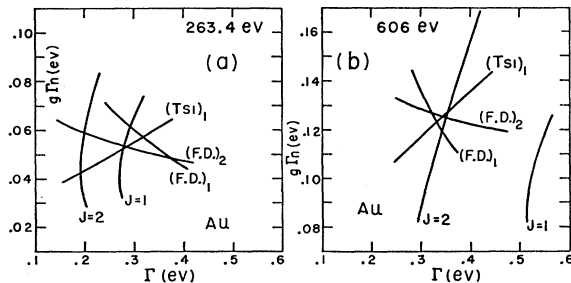Using these definitions, the $p$-wave match in Fig. 5



FIG. 12. Examples showing the analysis for the Au levels at 263.4 ev and 606 ev. These examples indicate the consistency between the flat detector data (F.D.) and the self-indication data. All of the level parameters are obtained even though $(T_{SI})_2$ is too small to be accurately employed. Figure 12(a) indicates a case where the self-indication data alone are not sufficient to determine $g\Gamma_n$ to within $\sim15\%$ since the two implied values of $\Gamma_\gamma$ are both reasonable.

gives

$$S_1 = (1.7 \pm 0.8) \times 10^{-4}. \qquad (8a)$$

If only $p_{\frac{1}{2}}$ induced levels are present, this implies

$$(S_1)_{\frac{1}{2}} = (4.1 \pm 2.4) \times 10^{-4}. \qquad (8b)$$

These results are in reasonable agreement with other evidence.[5]

## B. Gold

Figure 7 shows the results of the $D$-only, $(D+T_1)$, and $(D+T_2)$ self-indication measurements on Au. The flat detector transmission measurements are not shown but were very useful for the analysis. The results for the level positions and the values of level parameters are given in Table II. Figure 8 shows the running sum of the number of observed levels vs $E$. If the upward excursion between 600 and 900 ev is followed in obtaining the best $\bar{D}$, one obtains $\bar{D}=15.8$ ev, corresponding to the upper line in Fig. 8. A choice of $\bar{D}=16.8$ ev, however, gives a better fit below 600 ev and is never far from the experimental sum as high as 1600 ev.

Figure 9 gives the integral distribution of $(2g\Gamma_n{}^0)$ values below 800 ev as a function of $(2g\Gamma_n{}^0)^{\frac{1}{2}}$. If $\sum(2g\Gamma_n{}^0)$ is kept fixed, but it is assumed that some weak levels may have been missed, it is found that a good fit over most of the region is obtained by assuming that 2 weak levels were missed. A single-population Porter-Thomas function is used to compare with the experimental distribution. Figure 10 shows $\sum(2g\Gamma_n{}^0)$ vs $E$ to 940 ev. The best-fit value for $S_0 = \langle g\Gamma_n{}^0 \rangle/\bar{D}$ $= (1.5 \pm 0.3) \times 10^{-4}$.

Figure 11 shows the observed distribution of the 88 level spacings between the levels at 4.9 ev and 1566 ev. An assumed random distribution of level spacings, normalized to 88 spacings, predicts significantly more small and large spacings, and fewer average sized spacings than are observed. A single population Wigner distribution function has the form $P(x)dx = x \exp(-x^2/$

2)$dx$, where $x$ is proportional to the level spacing $s$. This predicts fewer small and large spacings than observed, and more average sized spacings. If we really believed that the random distribution function applied to Au, we would say that many small spacings had been missed. The "random" curve in Fig. 11 is constructed assuming that 27 small spacings were missed and is started at $-27$ for zero spacing. Similarly, if one

believed that the Wigner single population function applied, one might argue that some structures which have been interpreted as due to two incompletely resolved levels were actually single. Although this is considered unlikely, the Wigner single population curve in Fig. 11 is based on 80 spacings and starts at $+8$ for zero spacing. Since Au has $I = \frac{3}{2}$, the $J = 1$ levels are

TABLE II. Resonance parameters for Au. The values for the 4.9-ev level are from BNL-325. All other values are from the present measurements. The $J$ values in parentheses are regarded as less reliable than the others.

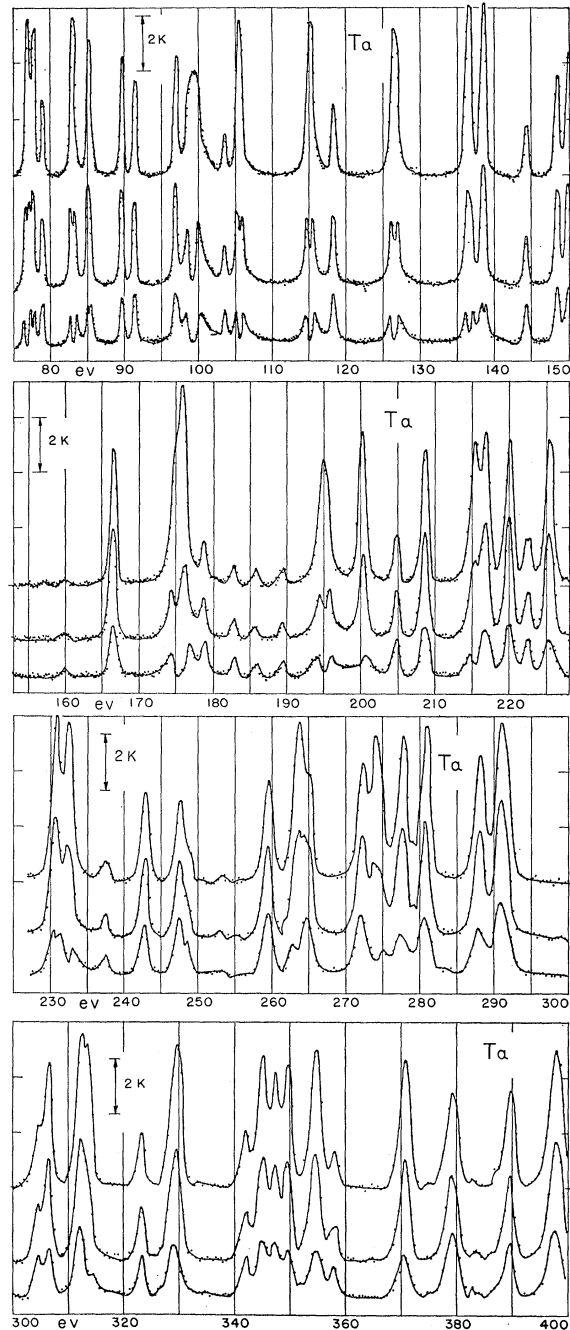| $E_0$ (ev) | $2g\Gamma_n$ ($10^{-3}$ ev) | $\Gamma_\gamma$ ($10^{-3}$ ev) | $J$ | $2g\Gamma_n{}^0$ ($10^{-3}$ ev) |
|---|---|---|---|---|
| 4.906±0.010 | 19.5±0.5 | 124±3 | 2 | 8.80±0.23 |
| 46.7±0.08 | 0.11±0.02 | | | 0.016±0.003 |
| 58.2±0.1 | 4.7±0.7 | 143±30 | | 0.62±0.09 |
| 60.3±0.1 | 95±15 | 120±20 | (2) | 12.2±1.9 |
| 78.7±0.2 | 13±1 | 145±15 | | 1.47±0.11 |
| 107.3±0.2 | 9.3±0.5 | 165±15 | | 0.90±0.05 |
| 122.6±0.2 | 0.8±0.1 | | | 0.072±0.009 |
| 144.8±0.3 | 6.5±0.6 | 190±20 | | 0.54±0.05 |
| 151.8±0.3 | 29±3 | 179±30 | 2 | 2.36±0.24 |
| 163.6±0.3 | 40±10 | | | 3.12±0.78 |
| 165.6±0.3 | 12±3 | | | 0.93±0.23 |
| 190.7±0.4 | 27±4 | 189±20 | (1) | 1.95±0.29 |
| 209.6±0.4 | 0.72±0.07 | | | 0.050±0.005 |
| 241.4±0.5 | 85±6 | 185±20 | 2 | 5.5±0.4 |
| 256.2±0.5 | 0.6±0.1 | | | 0.037±0.006 |
| 263.4±0.5 | 113±6 | 136±15 | 1 | 6.95±0.37 |
| 275.0±0.5 | 5.0±1.0 | 127±50 | | 0.30±0.06 |
| 294.5±0.6 | 400±60 | 250±80 | | 23.3±3.5 |
| 330.5±0.7 | 200±100 | | | 11.0±5.5 |
| 332.5±0.7 | 60±30 | | | 3.3±1.6 |
| 357 ±0.7 | 51±3 | 177±25 | 2 | 2.70±0.16 |
| 373 ±0.7 | 115±15 | | | 5.95±0.78 |
| 377 ±0.8 | 12±6 | | | 0.62±0.31 |
| 384 ±0.8 | 90±9 | | | 4.60±0.46 |
| 403 ±0.8[a] | 26±4 | 590±80 | | 1.30±0.20 |
| 442 ±0.9 | 230±30 | 280±70 | (1) | 10.9±1.4 |
| 453 ±0.9 | 90±12 | 250±50 | (1) | 4.23±0.56 |
| 479 ±1.0 | 376±40 | 180±70 | 2 | 17.2±1.8 |
| 492 ±1.0 | 45±10 | | | 2.03±0.45 |
| 496 ±1.0 | 15±4 | | | 0.67±0.18 |
| 538 ±1.1 | 39±5 | 280±50 | | 1.68±0.22 |
| 551 ±1.1 | 36±4 | 282±40 | | 1.53±0.17 |
| 565 ±1.1 | 3.3±0.4 | | | 0.139±0.017 |
| 583 ±1.2 | 370±50 | | | 15.3±2.1 |
| 590 ±1.2 | 30±15 | | | 1.23±0.62 |
| 606 ±1.2 | 248±20 | 140±15 | 2 | 10.1±0.8 |
| 621 ±1.2 | 83±8 | 160±40 | (1) | 3.32±0.32 |
| 628 ±1.3 | 60±20 | | | 2.40±0.80 |
| 632 ±1.3 | 35±15 | | | 1.39±0.60 |
| 644 ±1.3 | 490±60 | 270±100 | (1) | 19.3±2.4 |
| 664 ±1.4 | 6±1 | | | 0.23±0.04 |
| 691 ±1.4 | 10±3 | | | 0.38±0.11 |
| 702 ±1.5 | ~400 | | | ~15.1 |
| 706 ±1.5 | ~240 | | | ~9.0 |
| 721 ±1.5 | 108±12 | 210±35 | 2 | 4.0±0.4 |
| 743 ±1.6 | 11±3 | | | 0.40±0.11 |
| 766 ±1.6 | 320±40 | 154±60 | 1 | 11.6±1.4 |
| 781 ±1.7 | 148±40 | | | 5.3±1.4 |
| 791 ±1.8 | 125±25 | 170±40 | | 4.4±0.9 |
| 803 ±1.8 | 214±43 | 217±100 | (1) | 7.55±1.52 |
| 819 ±1.8 | ~40 | | | ~1.4 |
| 825 ±1.9 | ~150 | | | ~5.2 |
| 831 ±1.9 | ~150 | | | ~5.2 |
| 871 ±2.0 | 16±4 | 150±70 | | 0.54±0.14 |
| 886 ±2.1 | 65±10 | 125±50 | | 2.18±0.34 |
| 940 ±2.3 | 540±90 | ~110 | (2) | 17.6±2.9 |

[a] Probably double.



FIG. 13. Self-indication data for Ta similar to that of Fig. 2 for Ag. The $D$, $T_1$, and $T_2$ samples have $n^{-1}$ of 140, 700, and 140 barns/atom, respectively.

TABLE III. Resonance parameters for Ta. Level parameters below 65 ev are from BNL-325.

| $E_0$ (ev) | $2g\Gamma_n$ ($10^{-3}$ ev) | $\Gamma_\gamma$ ($10^{-3}$ ev) | $2g\Gamma_n^0$ ($10^{-3}$ ev) | $E_0$ (ev) | $2g\Gamma_n$ ($10^{-3}$ ev) | $\Gamma_\gamma$ ($10^{-3}$ ev) | $2g\Gamma_n^0$ ($10^{-3}$ ev) |
|---|---|---|---|---|---|---|---|
| 4.28±0.01 | 4.05±0.125 | 56±6 | 1.97±0.056 | 178.7 ±0.4 | 1.0±0.5 | | 0.075±0.04 |
| 10.34±0.05 | 4.05±0.125 | 61±6 | 1.26±0.034 | 182.7 ±0.4 | 0.85±0.11 | | 0.063±0.008 |
| 13.95±0.10 | 1.12±0.03 | 52±3 | 0.30±0.01 | 185.8 ±0.4 | 0.60±0.10 | | 0.044±0.007 |
| 18.6 ±0.2 | 0.78±0.09 | 85±20 | 0.18±0.02 | 189.5 ±0.4 | 0.70±0.11 | | 0.051±0.008 |
| 20.4 ±0.1 | 1.08±0.04 | 64±5 | 0.24±0.01 | 195.0 ±0.5 | 74±10 | | 5.3±0.7 |
| 22.8 ±0.1 | 0.24±0.02 | 51±14 | 0.050±0.004 | 200.5 ±0.4 | 40±5 | 63±10 | 2.8±0.4 |
| 24.1 ±0.1 | 6.4±0.2 | 61±4 | 1.30±0.04 | 204.9 ±0.4 | 2.9±0.3 | | 0.20±0.02 |
| 29.9 ±0.1 | 0.24±0.04 | 60±20 | 0.044±0.007 | 208.5 ±0.4 | 13±2 | | 0.90±0.14 |
| 35.2 ±0.3 | 13.9±0.5 | 61±6 | 2.34±0.08 | 215.5 ±0.4 | 43±6.5 | 65±16 | 2.93±0.45 |
| 35.9 ±0.3 | 16.6±0.6 | 69±7 | 2.78±0.10 | 217.0 ±0.4 | 15±6 | | 1.02±0.4 |
| 39.2 ±0.2 | 50.2±1.0 | 64.3±3.3 | 7.98±0.225 | 220.0 ±0.4 | 17.5±2.6 | | 1.18±0.18 |
| 49.1 ±0.3 | 1.09±0.09 | 55±15 | 0.16±0.01 | 222.5 ±0.5 | 1.8±0.36 | 52±13 | 0.120±0.024 |
| 55.9 ±0.8 | 0.2±0.1 | | 0.03±0.01 | 225.5 ±0.5 | 28±4.2 | | 1.86±0.28 |
| 57.5 ±0.4 | 0.3±0.1 | | 0.04±0.02 | 230.8 ±0.5 | 32±8 | | 2.1±0.5 |
| 63.0 ±0.4 | 6.2±0.3 | 61±7 | 0.79±0.04 | 232.5 ±0.5 | 65±16 | | 4.3±1.1 |
| 76.9 ±0.2 | 11±1.7 | 69±20 | 1.25±0.19 | 237.5 ±0.5 | 1.4±0.3 | | 0.09±0.02 |
| 77.7 ±0.2 | 5.5±1.1 | | 0.62±0.12 | 243.0 ±0.5 | 10.0±2.0 | | 0.64±0.13 |
| 79.0 ±0.2 | 2.2±0.4 | | 0.22±0.03 | 247.0 ±0.5 | 7.3±1.1 | | 0.47±0.07 |
| 83.0 ±0.2 | 16±2 | 58±8 | 1.76±0.22 | 248.5 ±0.5 | 1.4±0.4 | | 0.089±0.031 |
| 85.2 ±0.2 | 4.4±0.4 | 58±12 | 0.48±0.05 | 253.3 ±0.5 | 0.3±0.06 | | 0.019±0.004 |
| 85.8 ±0.2 | ~0.3 | | ~0.03 | 259.5 ±0.5 | 11.0±1.7 | | 0.685±0.10 |
| 89.7 ±0.2 | 3.5±0.3 | 55±18 | 0.37±0.03 | 260.0 ±0.5 | 0.6±0.3 | | 0.037±0.02 |
| 91.5 ±0.2 | 2.4±0.2 | | 0.25±0.03 | 263.5 ±0.5 | 95±24 | | 5.86±1.50 |
| 97.1 ±0.2 | 4.0±1 | | 0.41±0.1 | 264.5 ±0.5 | 14±4 | | 0.86±0.26 |
| 99.4 ±0.2 | 125±25 | 50±15 | 12.6±2.5 | 272.2 ±0.5 | 14±4 | | 0.85±0.26 |
| 103.6 ±0.2 | 1.0±0.2 | | 0.10±0.02 | 274.0 ±0.5 | 100±25 | | 6.05±1.5 |
| 105.6 ±0.2 | 32±3 | 46±10 | 3.1±0.3 | 277.5 ±0.6 | 25±8 | | 1.50±0.45 |
| 115.2 ±0.2 | 48±5 | 39±12 | 4.5±0.47 | 280.5 ±0.6 | 30±6 | | 1.79±0.36 |
| 118.4 ±0.2 | 2.3±0.4 | | 0.21±0.037 | 288.2 ±0.6 | 27±6 | | 1.59±0.32 |
| 126.6 ±0.2 | 45±4 | 53±10 | 4.0±0.36 | 291.0 ±0.6 | ~18 | | ~1.06 |
| 136.6 ±0.3 | 25±5 | 55±14 | 2.1±0.4 | 291.5 ±0.6 | ~18 | | ~1.06 |
| 138.5 ±0.3 | 13±2 | 66±20 | 1.1±0.17 | 304.5 ±0.6 | 2.7±0.7 | | 0.155±0.04 |
| 144.3 ±0.3 | 1.7±0.3 | | 0.14±0.025 | 306.5 ±0.6 | 31±8 | | 1.77±0.45 |
| 148.5 ±0.3 | 4.8±0.5 | | 0.394±0.041 | 312.0 ±0.6 | 25±6 | | 1.41±0.35 |
| 149.5 ±0.3 | 6.0±0.6 | | 0.49±0.05 | 313.8 ±0.6 | 40±10 | | 2.25±0.56 |
| 160.0 ±0.3 | 0.35±0.08 | | 0.028±0.006 | 323.0 ±0.6 | 6.0±0.9 | | 0.334±0.05 |
| 166.5 ±0.3 | 9.0±1.0 | | 0.70±0.08 | 329.0 ±0.7 | 25±12 | | 1.38±0.7 |
| 175.2 ±0.3 | ~90 | | ~6.8 | 329.5 ±0.7 | 45±22 | | 2.48±1.2 |
| 176.0 ±0.4 | ~50 | | ~3.8 | | | | |
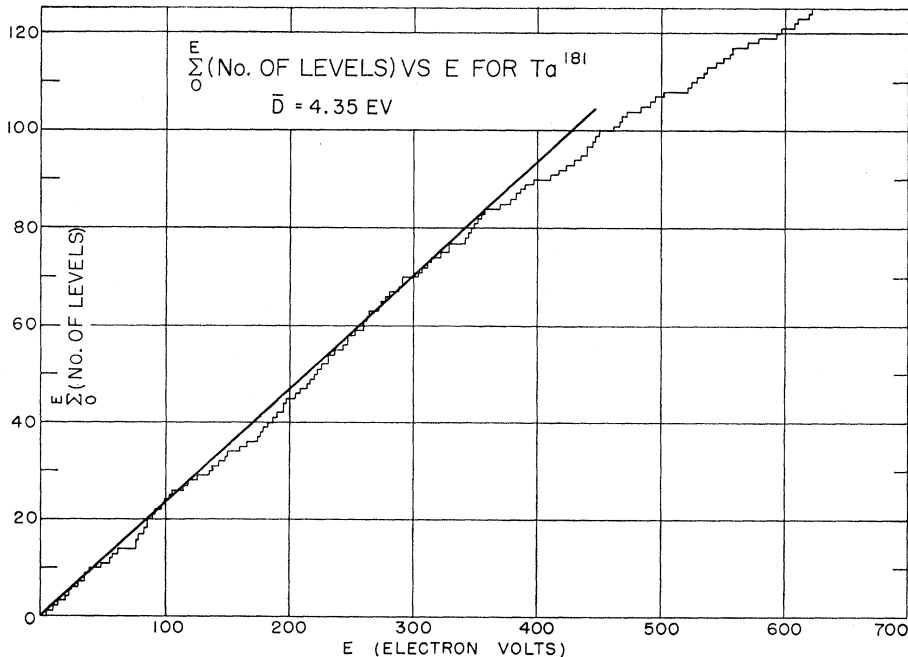


FIG. 14. The number of levels to energy $E$ vs $E$ for Ta. There is evidence of a significant loss of levels above ~350 ev. The line indicates $\bar{D}=4.35$ ev.
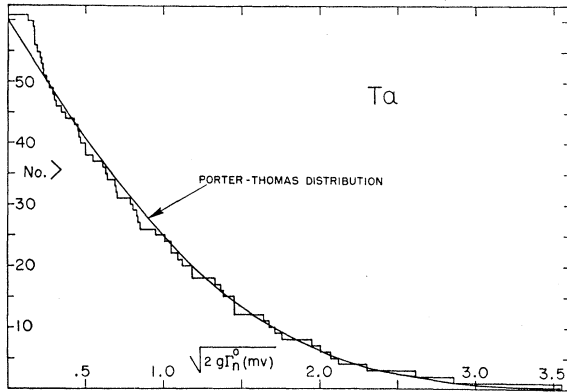
Fig. 15. Integral distribution of the reduced width amplitudes for Ta. A good fitting Porter-Thomas distribution was obtained by normalizing to one less than the observed number of levels. This reflects the apparent slight excess of small $(2g\Gamma_n^0)^{\frac{1}{2}}$ values.

expected to have a Wigner (single) spacing distribution which is randomly positioned with respect to the Wigner (single) $J=2$ spacing distribution. If a $(2J+1)$ level density factor applies, $\frac{3}{8}$ of the levels should have $J=1$ and $\frac{5}{8}$ of the levels have $J=2$. Using this assumption we show the expected spacing distribution for the cases where 2 or 6 small spacings are assumed missed. Either of these choices gives excellent agreement with the experimental distribution over most of its range and represent reasonable estimates of the number of small spacings missed.

The theory applicable for the case of two randomly superimposed populations is outlined below. Let $P_1(s)ds$ and $P_2(s)ds$ be the separate spacing distribution functions for the separate populations and $P(s)ds$ be that for the two randomly superimposed. Then it is readily shown that

$$P(s)ds = \frac{ds}{(D_1+D_2)}\left\{ P_1(s)\int_0^\infty xP_2(x+s)dx \right.$$

$$+P_2(s)\int_0^\infty xP_1(x+s)dx$$

$$\left. +2\int_0^\infty P_1(x+s)dx\int_0^\infty P_2(x+s)dx \right\}; \quad (9)$$

where $D_1$ and $D_2$ are the separate average spacings. Let $P_1$ and $P_2$ be separate Wigner (single) distributions of the form $P_1(a)da = a\exp(-a^2/2)da$ and $P_2(b)db = b\exp(-b^2/2)db$, where $a=(\pi/2)^{\frac{1}{2}}s/D_1 = n(n+1)^{-1}(\pi/2)^{\frac{1}{2}}s/D$ and $b=(\pi/2)^{\frac{1}{2}}s/D_2 = (n+1)^{-1}(\pi/2)^{\frac{1}{2}}s/D$. The factor $n$ represents the ratio $D_2/D_1$ of the two average level spacings. The integral of the level spacing has a simpler form than $P(s)$ itself and may be written

$$\int_0^s P(s)ds = 1 - (n+1)^{-1}\{n\exp(-a^2/2)[1-2\operatorname{erf}(b)]$$

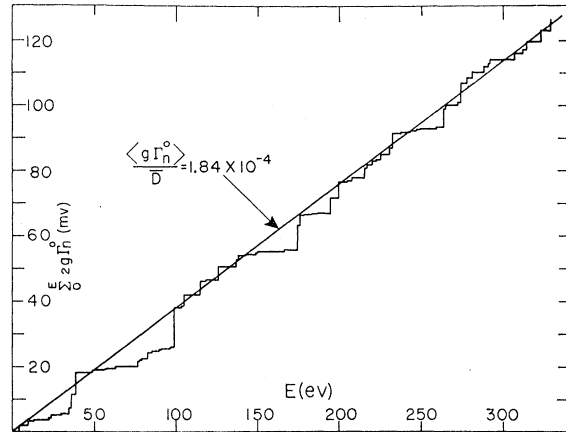$$+\exp(-b^2/2)[1-2\operatorname{erf}(a)]\}, \quad (10)$$



Fig. 16. The sum $E=0$ to $E$ of the $2g\Gamma_n^0$ values for Ta to 330 ev. The slope divided by 2 determines the Ta strength function. The large value, $1.84\times10^{-4}$ reflects a resonance in the $s$-wave strength function.

where

$$\operatorname{erf}(x) \equiv (2\pi)^{-\frac{1}{2}}\int_0^x \exp(-y^2/2)dy \quad (11)$$

is the usual tabulated function. For $a=b$ an obvious simplification results. The separation of the curves for $n=1$ and $n=2$ is much smaller than that of either from the random or Wigner (single) curve.

Figure 12(a) and (b) show the analyses for the 263.4-ev and 606-ev levels where $J=1$ and $J=2$, respectively, are clearly favored. These are relatively strong levels where $(T_{SI})_2$ is too near to zero to be useful. Note that the $(T_{SI})_1$ curve, in each case, is consistent with the thin and thick flat detector transmission results. The curves $J=1$ and $J=2$ are based on the total number of counts $C$ above background in the $D$-only resonance peak together with the $S_a$ value. The level at 403 ev, when treated as single, gives $\Gamma_\gamma \approx 0.60$ ev and is probably due to two superimposed levels.

Inspection of Table II shows large fluctuation in the values of $\Gamma_\gamma$ even when what are believed to be realistic uncertainties in the measurements are considered.

## C. Tantalum

The Ta self-indication results to 400 ev are shown in Fig. 13 and the level parameter results are given in Table III. The results for the levels below 65 ev are from BNL-325. Figure 14 shows the running sum of the number of observed levels as a function of $E$. It suggests that almost all levels are counted below 350 ev.

The integral distribution of $(2g\Gamma_n^0)$ values vs $(2g\Gamma_n^0)^{\frac{1}{2}}$ is shown in Fig. 15 compared with a single Porter-Thomas distribution normalized to 1 less level than observed. Figure 16 shows $\sum(2g\Gamma_n^0)$ vs $E$ and gives

$$S_0 = (1.84\pm0.34)\times10^{-4}.$$

RANDOM (90) - 14

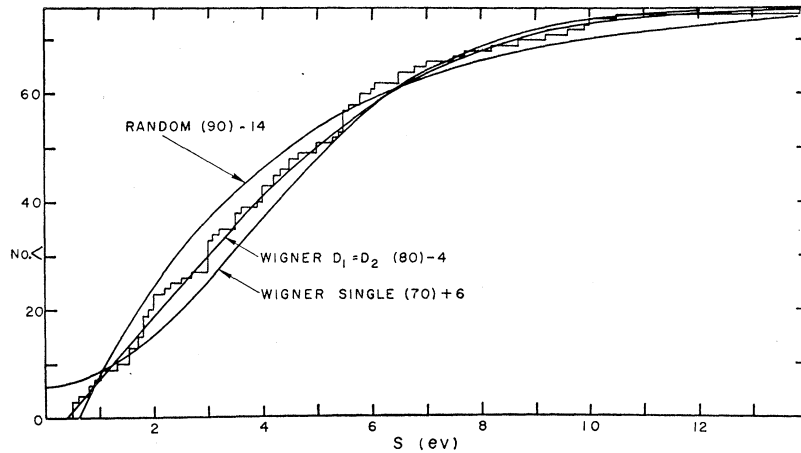WIGNER $D_1 = D_2$ (80)-4

WIGNER SINGLE (70) +6

S (ev)

Fig. 17. Integral distribution of the 76 observed level spacings for Ta to 330 ev. As in the similar plot for Au, Fig. 11, each theoretical curve has the total number of levels adjusted for best fit. The best fitting two population $D_1 = D_2$ Wigner distribution is normalized to 80 total spacings so it intercepts the $y$ axis at $-4$.

Figure 17 shows the distribution of level spacings. Since $I = \frac{7}{2}$, a two-population fit was made using $D_1 = D_2$ in Eq. (10). The theoretical fits were made using the same reasoning as for the Au fit in Fig. 11. The "random" curve was based on 14 extra spacings with an intercept of $-14$ at $s = 0$. The Wigner (single) distribution was based on 6 fewer spacings with an intercept of $+6$ at $s = 0$. The excellent fit Wigner $D_1 = D_2$ distribution was based on 4 extra spacings with an intercept of $-4$ at $s = 0$. It is plausible to assume that this many spacings were missed, but the number missed is probably not much larger than this.

## ACKNOWLEDGMENTS